Combining Perfluorocarbon and Superparamagnetic Iron-oxide Cell Labeling for Improved and Expanded Applications of Cellular MRI

T. Kevin Hitchens[1,*], **Li Liu**[1], **Lesley M. Foley**[1], **Virgil Simplaceanu**[1,2], **Eric T. Ahrens**[1,2,†], and **Chien Ho**[1,2]

[1]Pittsburgh NMR Center for Biomedical Research, Carnegie Mellon University, Pittsburgh, PA 15213 USA

[2]Department of Biological Sciences, Carnegie Mellon University, Pittsburgh, PA 15213 USA

Abstract

Purpose—The ability to detect the migration of cells in living organisms is fundamental in understanding biological processes and important for the development of novel cell-based therapies to treat disease. MRI can be used to detect the migration of cells labeled with superparamagnetic iron-oxide (SPIO) or perfluorocarbon (PFC) agents. In this study, we explored combining these two cell-labeling approaches to overcome current limitations and enable new applications for cellular MRI.

Methods—We characterized ^{19}F-NMR relaxation properties of PFC-labeled cells in the presence of SPIO and imaged cells both *ex vivo* and *in vivo* in a rodent inflammation model to demonstrate selective visualization of cell populations.

Results—We show that with UTE3D, RARE and FLASH ^{19}F images one can uniquely identify PFC-labeled cells, co-localized PFC- and SPIO-labeled cells, and PFC/SPIO co-labeled cells.

Conclusion—This new methodology has the ability to improve and expand applications of MRI cell tracking. Combining PFC and SPIO strategies can potentially provide a method to quench PFC signal transferred from dead cells to macrophages, thereby eliminating false positives. In addition, combining these techniques could also be used to track two cell types simultaneously and probe cell-cell proximity *in vivo* with MRI.

Keywords

Cell Tracking; MRI; Superparamagnetic Iron-oxide; Perfluorocarbon

Introduction

The ability to observe cell migration in living organisms is key to understanding biological processes and developing novel cellular therapies for a large number of diseases that

[*]To whom correspondence should be addressed: T. Kevin Hitchens, PhD, MBA, Assistant Director, Pittsburgh NMR Center for Biomedical Research, Carnegie Mellon University, 4400 Fifth Avenue, Pittsburgh PA 15213.
[†]Current address: Department of Radiology, University of California at San Diego, San Diego, CA 92093 USA

continue to elude traditional therapeutic approaches. There are several imaging modalities that are able to track cells *in vivo*, such as MRI, single-photon emission tomography (SPECT), or bioluminescence and fluorescence imaging (1–4). Of these, MRI has the broadest application because it is useful clinically, is not limited by depth of penetration, has a moderately high resolution, and does not rely on a radioactive tracer.

To make cells visible by MRI, they are labeled with an agent that provides image contrast or a unique magnetic resonance signal. In principle, any agent expressed or loaded into a cell that can affect the signal or relaxation properties of the surrounding water can be used for cellular MRI. Many studies rely on nanometer-sized or micron-sized superparamagnetic iron-oxide (SPIO) particles to track cells by MRI. SPIO loaded into cells can affect the surrounding water T_1 and T_2, but often T_2* contrast is used because the magnetic-field gradients generated by the SPIO can extend far beyond the boundary of the cell, causing a so-called “blooming effect”. In fact, in some cases, single cells can be detected in images collected at far less than cellular resolution (5–7).

Recently, there has been increased interest in the use of perfluorocarbon (PFC) nanoemulsions as tracer agents for MRI cell tracking (8). Fluorine-19 (^{19}F) is the only abundant and stable isotope of fluorine. It is an NMR active, spin-1/2 nucleus that has a gyromagnetic ratio similar to ^{1}H. In biological systems, fluorine has a very low natural abundance, mainly in the form of fluoride; thus, any fluorine-containing molecules introduced can provide a unique signal for magnetic resonance spectroscopy and imaging. For cell tracking, PFC molecules with a large number of chemically equivalent fluorine atoms are formulated into nanoemulsions for cell labeling (9). Because there is a lack of background signal, the presence of even low fluorine signal intensity (SNR>2) can be used to localize the labeled cells *in vivo*, and, importantly, the magnitude can be directly related to the number of cells (10). A standard ^{1}H image can then be used to place the labeled cells in anatomical context.

Current MRI cell tracking methods using labeling agents have several limitations. One limitation is the inability to distinguish live cells from dead cells that have transferred their labeling agent to macrophages *in vivo* (11, 12), thereby giving rise to the possibility of false positive signals. Another limitation is that, in general, only a single labeled cell type (or cell population) can be uniquely tracked in the same image voxel with MRI. By combining PFC and SPIO labeling, we aimed to develop a methodology able to overcome these limitations in order to improve and expand the applications of cellular MRI.

In this study, we explored the effects of SPIO cellular contrast agents on properties of PFC reagents used for cell labeling. We found that an intracellular co-label of SPIO nanoparticles significantly reduced the PFC ^{19}F T_2. However, when cell populations were labeled with a single agent, the ^{19}F T_2 of PFC-labeled cells was largely unaffected by adjacent SPIO-labeled cells. By taking advantage of the ^{19}F relaxation properties, we demonstrated that by combining PFC and SPIO reagents, one can uniquely detect PFC-labeled cells, PFC-labeled cells co-localized with SPIO-labeled cells, and SPIO/PFC co-labeled cells. This methodology has the potential to provide a way to quench PFC signal released to

macrophages from dead cells *in vivo*, and provide a method to track two (or more) cell populations simultaneously.

Methods

Cellular MRI Reagents

PFC cell labeling reagents were obtained from a commercial source (Celsense, Inc., Pittsburgh, PA). Two PFC reagents were used in this study, both containing the same MRI-active molecule; one is an emulsion formulated for cell labeling in culture (Cell Sense, product # CS-1000-ATM), and the other formulated for direct intravenous administration for labeling immune cells *in situ* (V-Sense, product # VS-1000 H). Two different SPIO nanoparticles were also used in this study. Molday ION was obtained from BioPal (Worchester, MA), and is comprised of 30 nm dextran-coated SPIO particles with a transverse relaxivity (r_2) of 70.6 $mM^{-1}{\cdot}sec^{-1}$ for water at 0.47 T. For cell labeling in culture, Molday ION C6Amine was used. ITRI-IOP was a gift from Shian-Jy Wang (Industrial Technology Research Institute, Hsinchu, Taiwan), and is comprised of a polyethylene glycol coated SPIO particle with a hydrodynamic diameter of 70 nm and an r_2 of 240 mM^{-1} sec^{-1} at 0.47 T (13, 14). Micron-sized iron-oxide particles (MPIO), product number MC03F, were obtained from Bangs Laboratories (Fishers, IN). These particles consist of a 0.9 μm styrene-divinylbenzene polymer sphere loaded with SPIO. These particles have a relatively low r_2, of 35 mM^{-1} sec^{-1} (13), but have a very high r_2*, i.e. similar particles are reported to have r_2* of 356 mM^{-1} sec^{-1} at 4.7 T (15).

NMR and MRI equipment

All ^{19}F NMR and MRI measurements were made at 7 Tesla. ^{19}F NMR measurements of cell preparations were performed at 282 MHz on a Bruker DRX300WB spectrometer (Bruker Biospin, Billerica MA) with a 10 mm dual $^{19}F/^{1}H$ probe at ambient temperature. Imaging was carried out using a 7 Tesla, 21 cm, Bruker Biospec AVANCE 3 scanner equipped with a 12 cm B-GA12S2 gradient set and a 35-mm $^{1}H/^{19}F$ double-resonance birdcage coil (Rapid International, Columbus, OH).

^{19}F-NMR relaxation properties of PFC/SPIO nanoparticle mixtures

Aqueous mixtures of 20% VS-1000 and Molday ION were prepared with iron concentrations of 0, 0.4, 2.0, 4.0, and 20 μg/mL. The effect of SPIO concentration on ^{19}F T_1 and T_2 relaxation was demonstrated by MRI. The ^{19}F T_1 was determined using a DESPOT1 analysis (16) by fitting signal intensities obtained from eleven 3-dimensional Ultra-short TE (UTE3D) images with different flip angles, ranging from 2° to 22°. Other parameters included a 3D matrix of 80 points, a resolution of 0.75×0.75×1.5 mm, TR/TE = 8 ms/20 μs, and NA = 24. T_2 was estimated from a monoexponential fit of the signal decay from a series of RARE (Rapid Acquisition with Relaxation Enhancement) images with echo times ranging from 10 to 150 ms, TR = 1000, RARE Factor = 2, NA = 8, and the same resolution as above.

Preparation of PFC- and USPIO-labeled Cells

To demonstrate ^{19}F nuclear relaxation properties and selective imaging of PFC-labeled cell populations, a fetal skin-derived dendritic cell (FSDC) line was labeled with PFC and/or SPIO reagents. FSDCs were a gift from Ricciardi-Castagnoli (17). FSDCs were cultured as a monolayer in 10 cm plates in complete RPMI 1640 medium containing 10% fetal bovine serum (FBS), 100 μg/mL streptomycin, 100 U/mL penicillin, and 2 mM glutamine at 37 °C, as described elsewhere (18). At ~90% confluence, FSDCs were incubated with the SPIO particles, PFC emulsion, or a mixture of both SPIO and PFC in culture medium for 18 hr. The concentrations of the MRI contrast agents were as follows: ITRI-IOP (10 or 25 μg Fe/mL), Molday ION (35 or 70 μg Fe/mL), MPIO (10 or 20 μg Fe/mL), and PFC (CS-1000ATM at 8 mg/mL). After the incubation, FSDCs were washed 3x with phosphate-buffered saline (PBS) to remove any excess labeling agent. FSDCs were then incubated with 5 mL of trypsin-EDTA at 37 °C for 5 min and harvested by centrifugation (300×g for 7 min). The cells were then washed twice with PBS. The cells were counted and the number of dead cells was determined to be less than 10% using the Trypan Blue exclusion assay. The intracellular iron concentrations were determined analytically by inductively coupled plasma mass spectrometry (ICP-MS) (PerkinElmer NexION300X, Waltham, MA) with a known number of cells compared to a calibration curve. The cells were fixed with 2% paraformaldehyde for 24 hr, then stored in PBS.

Three types of cell phantom samples were prepared: PFC-labeled cells as control, mixed populations of PFC-labeled and SPIO-labeled cells, and co-labeled PFC/SPIO cells. In the latter two cases, a few samples with different intracellular concentrations of iron were made. For all samples, a total of 6×10^6 labeled FSDCs were prepared as a cell pellet in a 0.4 mL narrow microcentrifuge tube (FisherBrand Cat. #02-681-229). For the mixed population, equal number of cells were evenly mixed (3×10^6 SPIO-labeled cells and 3×10^6 PFC-labeled cells) prior to centrifugation.

^{19}F-MRI of Cell Pellets

The cell pellets were imaged with ^{19}F MRI using 3 different sequences: a UTE3D, RARE, and FLASH (Fast Low-Angle snapSHot), for spin density-weighted images, T_2-weighted images and T_2*-weighted images, respectively. The UTE3D was collected with the following parameters: TR/TE = 10/0.015 ms, 10° FA, 28,733 projections, NA = 48, and an isotropic matrix of 96 points with a resolution 0.5×0.5×2 mm. The RARE images were collected with TR/TE = 2000/6 ms, 96×96 matrix, 4.8 cm FOV, 8mm slice thickness (to contain the entire cell pellet), NA = 64, RARE factor = 2, and 8 echo images for effective echo times of 12, 36, 60, 84, 108, 156, and 180 ms. FLASH imaging used a TR/TE = 100/1 ms, 48×16 matrix, 4.8 cm FOV, 30° FA, and NA = 1024. For illustration of cell population selection, images from cell pellets with PFC-only labeled cells, a mixed population of PFC and ITRI-IOP-labeled cells (0.45 pg Fe/cell) and PFC/ITRI-IOP co-labeled cells (0.56 pg Fe/cell) were selected. The decay in signal intensity versus TE was plotted from the series of RARE images to measure the signal decay in the co-labeled population.

^{19}F-NMR Spectroscopy and Relaxometry

Following imaging, cell pellets were subjected to ^{19}F NMR spectroscopy. NMR spectra were collected on each sample to measure linewidth and peak position. Inhomogeneous line broadening in the cell pellets prevented accurate measurement of intracellular ^{19}F relaxation rates by spectroscopy, so cell pellets (~20 μL in volume) were then uniformly suspended in 80 μL of 1.0% low-melting-temperature agarose (Thermo Fisher Scientific Inc, Waltham, MA) and placed in shortened 5 mm borosilicate glass NMR tubes. For the 1D spectra, a 10 μs 45° pulse was used to collect 4 k points of the FID with a 120 ppm spectral width, using 8 to 32 averages and a recycle delay of 1 sec. T_2 was measured using the CPMG sequence (19, 20) with 9 μs 90° and 18 μs 180° pulses, and echo time of 1 ms; echoes were collected at multiples of 4 ms up to 800 ms. A 2-sec recycle delay was used to collect 8–32 averages depending on the sample. T_2 was determined with a 3-parameter monoexponential decay using XWIN NMR software (Bruker). T_1 was measured by saturation recovery using an aperiodic pulse train for saturation. For the samples with higher iron concentrations, rapid relaxation precluded the measurement of T_2 because the signal decayed before the formation of the first echo at 4 ms.

Electron Microscopy

Labeled FSDCs were fixed in 1% OsO_4 buffered with PBS for 15 minutes. The cells were washed with distilled water three times. The samples were dehydrated using a gradient series of ethanol and embedded in an Epon-Araldite resin. The samples were sectioned using a diamond knife on a Reichert-Jung Ultracut-E ultramicrotome. 100 nm sections were mounted onto copper grids and coated with carbon. The sections were imaged on a Hitachi 7100 transmission electron microscope.

Demonstration of in vivo feasibility

A mouse injury-inflammation model was used to demonstrate feasibility of generating and detecting different PFC/SPIO-labeled cell combinations *in vivo*. Male C57BL6 mice were obtained from Jackson Laboratories (Bar Harbor, ME) and allowed water and food *ad libitum*. Mice were induced with 2% isoflurane in air then intubated and mechanically ventilated with 70/30 O_2/$N_2$0 and 2% isoflurane. A femoral cut-down was then performed and sutured for the injury-induced inflammation model. By direct i.v. injection, we labeled macrophages *in situ* to generate three different cell populations: PCF-labeled cells, a mixture of PFC-labeled cells in proximity to SPIO-labeled cells, and PFC/SPIO co-labeled cells. One mouse was injected with 0.2 mL PFC (VS-1000) via the tail vein and imaged 5 days later to observe PFC-labeled cells. Imaging was followed with an injection of Molday ION (6 mg/kg) and scanned 48 hrs later (i.e., day 7 after injury) to observe PCF labeled cells in proximity to SPIO labeled cells. A second scheme was used to create a population of co-labeled PFC/SPIO cells. Following surgical injury, both the PFC (0.2 mL) and Molday ION (6 mg Fe/kg) were injected simultaneously via the tail vein. The mouse was allowed to recover and scanned 48 hrs later to match the time following SPIO injection from the above experiment.

For *in vivo* imaging, mice were re-anesthetized, intubated and mechanically ventilated as above. A reference standard containing PFC was placed near the injection site and the

mouse was positioned in the magnet. Anatomical ^{1}H images were collected using a RARE sequence with the following parameters, TR/TE = 4000/7 ms, RARE Factor = 8, 256×256 matrix, NA = 2, FOV = 48×48 mm, with a 2 mm slice thickness. As with the fixed cell samples, three different imaging sequences were used to collect the ^{19}F images, including RARE, with TR/TE = 4000/7 ms, RARE Factor = 4, 96×96 matrix, FOV = 48×48 mm, 8-echo images (effective echo times = 14, 42, 70, 98, 126, 154, 182, 210 ms), NA = 24, 15 slices with a 2 mm slice thickness, TA = 38 min, a FLASH sequence with TR/TE = 500/3 ms, 96×64 matrix, FOV = 48×32, NA = 48 and FA = 45°, TA = 25 min, and a 3D UTE with TR/TE = 8/0.02 ms, 80×80×80 matrix, 19,932 projections, FOV = 40×40×80 with a 1 mm effective slice resolution, TA = 63 min.

Results

^{19}F-NMR relaxation Properties of PFC/SPIO mixtures

The effect of SPIO nanoparticles on the PFC nanoemulsion ^{19}F nuclear magnetic relaxation is shown in Figure 1. Figures 1a and 1b show T_2 and spin-density-weighted images, respectively. For T_2-weighted scans, the signal intensity is clearly reduced for higher concentrations of SPIO, but signal from the UTE (Fig. 1b) appears constant. Figure 1C shows a plot of the relaxation rates ($1/T_N$) versus iron concentration. Longitudinal relaxation ($1/T_1$) is independent of iron concentration; however, transverse relaxation is strongly dependent. The ^{19}F transverse relaxivity (r_2) for Molday ION was measured to be 316 sec^{-1} mM^{-1} (5.56 sec^{-1} μg^{-1} mL) up to 4 μg Fe per mL. Rapid transverse relaxation in the 20 μg Fe/mL sample (98 ± 24 sec^{-1}) increased the error in the R_2 fit from a few percent to 24%. Including this value provides a similarly good linear regression (R^2=0.998) and yields an r_2 of 4.73 sec^{-1} μg^{-1} mL.

^{19}F-NMR PFC and SPIO labeled cells

To test the effects of intracellular SPIO particles and distant SPIO particles (in nearby cells) on the ^{19}F-NMR properties of PFC-labeled cells, we prepared PFC-labeled, SPIO labeled, and PFC/SPIO co-labeled cells with different SPIO particles and iron concentrations. For SPIO labeling, the cells were incubated with different concentrations of particles to prepare different labeling concentrations. The PFC ^{19}F T_1 in labeled cells was measured to be 495 ± 20 ms, and as with the mixtures of PFC and SPIO particles shown in Figure 1, there was no significant difference with the addition of SPIO-labeled cells or in co-labeled cells. The average ^{19}F T_1 of all the samples containing SPIO was 502 ± 27 ms. The other NMR properties of labeled cell mixtures suspended in agarose are shown in Table 1. For all samples containing SPIO, a small down-field shift in the resonance line was observed. The presence of SPIO in the samples also leads to inhomogeneous line broadening of the ^{19}F resonance. The broadening was modest for mixed populations of cells, increasing the initial ^{19}F linewidth of 200 Hz by 2- to 3-fold, with only a weak dependence on iron-concentration. For PFC/SPIO co-labeled cells, the ^{19}F linewidth increased significantly, to greater than 1 kHz, for the lowest iron concentration. The linewidth was also greatly dependent on the intracellular iron concentration, increasing the linewidth up to 7–8 kHz for the highest concentrations studied.

The presence of SPIO-labeled cells, containing either nanoparticles (ITRI-IOP or Biopal Molday ION) or micron-sized particles up to 4–6 pg Fe/cell, mixed equally with PFC-labeled cells, did not significantly affect the ^{19}F T_2. However, T_2 was significantly affected in the co-labeled cell populations. SPIO nanoparticles were very effective in shortening the intracellular PFC ^{19}F T_2. Only 0.59 pg Fe/cell of ITRI-IOP co-label was sufficient to reduce the relaxation time by over 90%. Molday ION had a similar effect; however, the lowest cellular concentration studied had 3 pg of iron, and, at this concentration, the transverse relaxation was too rapid to measure. Interestingly, similar iron concentrations of the MPIO co-label did not affect T_2 as strongly as the nanoparticles. For MPIO, 4.2 pg of iron only reduced the T_2 by half.

Electron Microscopy of PFC/SPIO Co-labeled Cells

Electron microscopy was used to examine the intracellular proximity between the PFC and either iron-oxide nanoparticles or micron-sized particles. Figure 2b shows TEM of an FSDC labeled with PFC. The PFC droplets appear as electron-sparse circular white spots that are not observed in unlabeled cells (Figure 2a). Figure 2c shows TEM of a PFC/MPIO co-labeled cell. The MPIO particle is clearly seen as a dark area of high electron density, and the MPIO particle is not in contact with the PFC droplets. Each MPIO particle contains about 0.5 pg of iron. In contrast, TEM of a co-labeled PFC/ITRI-IOP (Fig. 2d), shows the nanoparticles distributed between and in close proximity with the PFC droplets, presumably co-localized in macropinosomal compartments of the FSDCs (21).

^{19}F MRI of PFC and SPIO Labeled Cells

Figure 3 demonstrates the application of different imaging schemes (spin density-weighted imaging, T_2-weighted imaging, and T_2*-weighted imaging) to select for cell populations of PFC-labeled cells, mixtures of PFC-labeled and SPIO-labeled cells, and PFC/SPIO co-labeled cells. Only one cell pellet from each population is shown for illustration. A UTE3D (Fig. 3a) yields a PFC-density weighted image. The ultra-short TE of 20 μs provides a ^{19}F image of all PFC containing cell populations because the rapid read-out can image samples with short T_2 (or T_2*). However, the signal intensity will be affected as the T_2 approaches the echo time. RARE images were collected as a series of echo images with increasing echo times. The intensity can also be affected if the T_1 varies significantly between samples; however we confirmed with cells diluted in agarose that the PFC ^{19}F T_1 was approximately 500 ms for all samples investigated. Figure 3b shows the fourth image in the RARE series, with an effective TE of 84 ms, demonstrating negative selection of the short T_2, PFC/SPIO co-labeled, cell population. A plot of the normalized signal intensity versus effective echo time (Fig. 3d) illustrates the rapid decay of the co-labeled cell population, whereas the PFC-labeled cells and the mixture of PFC-labeled cells and SPIO-labeled cells had a similar and slower signal decay. A 3-parameter, monoexponential fit of the signal decay for the co-labeled cells yields a T_2 of 23 ms. This value is in good agreement with the T_2 of 20 ms obtained by NMR spectroscopy when these cells were diluted 5x in agarose (Table 1). The lower signal observed at the second echo image (TE= 36 ms) for the mixed population of PFC- and SPIO-labeled cells versus the PFC-only cell population may be a result of a small population of short T_2 PFC, due to tight packing and close proximity of some PFC-labeled

cells to SPIO-labeled cells in the pellet. Otherwise the T_2 observed for these two samples is similar, as evidenced by similar signal decay after the second point.

Figure 3c demonstrates T_2*-weighted imaging showing that samples containing SPIO, either co-labeled cells or mixed populations of PFC-labeled and SPIO-labeled cells, had a very short ^{19}F T_2*. Only signal from the PFC-only labeled cell population is visible. The cell pellet samples may also experience additional T_2* relaxation because of an inhomogeneous Bo field resulting from difficulty in shimming the magnetic field across the very small cell pellets.

In vivo MRI Proof-of-Concept for PFC cell Population Selection

Since it is well known that immune cells, predominantly macrophages, take up cellular MRI agents *in vivo* (22, 23), we used a simple mouse inflammation model and direct i.v. injection of PFC and/or SPIO nanoparticles to test the feasibility of detecting different PFC-labeled cell populations *in vivo*. The top row of images in Figure 4 (Figs. 4a - 4d), were taken from a mouse imaged 5 days following surgical injury and i.v. injection of PFC. We interrogated the ^{19}F images of the mouse to find clearly identifiable fluorine signal in lymph nodes and organs of the reticuloendothelial system. Figure 4a shows an overlay of a ^{19}F UTE3D image on the anatomical image. The two fluorine hot-spots in the center of the image are from the iliac lymph nodes. These signals are strong in the short-TE RARE, long-TE RARE and FLASH images (Figs. 4b – 4d, respectively), demonstrating PFC-labeled cells with a long T_2 and T_2*. Following the imaging session, the mouse was given an i.v. injection of Molday ION and then imaged 2 days later. We hypothesized that the SPIO nanoparticles would label a different population of macrophages that would then co-localize with the population of PFC-labeled cells. The second row of images in Fig.4 (e - h) show the corresponding UTE3D, short-TE RARE, long-TE RARE and FLASH images, respectively. The signal from the Long-TE RARE (Fig. 4g) is strong, suggesting a long ^{19}F T_2; however, the signals were absent in the FLASH image, demonstrating a short T_2*. The combination of a long ^{19}F T_2 and short T_2* suggests that we were successful in generating a mixed population of PFC-labeled cells and Molday ION-labeled cells *in vivo*. The reference was imaged near the end of the tube, so the signals are not strong and fade with T_2* weighting due to magnetic susceptibility differences at the edge of the reference.

To generate a co-labeled cell population *in vivo*, we repeated the experiment, but followed the surgical injury with a simultaneous injection of PFC and Molday ION (Fig.4i – 4l). In this experiment, we identified signal in the iliac bone marrow as shown in the composite ^{19}F UTE3D/anatomical image (Fig 4i). This signal was found in a short-TE RARE (Fig. 4j); however, it was not seen in the long-TE RARE (Fig. 4k) nor in the FLASH image (Fig. 4l). This combination of short T_2 and short T_2* suggests that we were successful in generating a co-labeled cell population *in vivo*. There is a smaller area of PFC signal observed for the surgical injury site in Fig 4i compared to Fig 4j, this discrepancy is due to the smaller slice thickness for the UTE3D (1mm vs. 2 mm for the RARE) and the image slice displayed being at the anterior edge of the surgical injury site.

Discussion

The use of MRI for tracking cell transplants *in vivo* is well established for preclinical studies and is gaining increased interest for clinical research and development. Both ^{19}F MRI to detect PFC-labeled cells and ^{1}H MRI image contrast techniques to detect the effect of SPIO-labeled cells on the surrounding water signal are powerful techniques to visualize the migration and accumulation of cells in deep tissues. However, they both share the potential problem of generating a false positive result if the label is transferred from dead cell transplants to macrophages *in situ*. This study was motivated by the need to find a solution to this major problem facing all MRI cell-tracking studies. Our approach was to explore the ability of SPIO to quench the PFC signal in a similar manner that SPIO is used to generate ^{1}H image contrast for cell tracking and we systematically tested this in solution, with labeled cell preparations, and *in vivo* using a mouse model.

There are several important findings in this work. First, we observed that the ^{19}F T_1 of PFC in the cell labeling nanoemulsion is not affected by iron concentration when mixed with SPIO nanoparticles. Second, we observed that the ^{19}F PFC T_2 is greatly reduced when the two reagents are closely coupled, for example in the case of a co-labeled cell. Further, we found that the PFC ^{19}F T_2 is largely unaffected when the SPIO-label is distant, as in the case of adjacent SPIO-labeled cells and PFC-labeled cells, but T_2* contrast can be used to detect cell-cell proximity in this case. Not only did our findings demonstrate the ability to achieve our goal of quenching PFC signal in SPIO co-labeled cells, these findings allowed us to detect and distinguish different mixtures of PFC and SPIO-labeled populations with ^{19}F MRI using UTE3D for ^{19}F-density weighted imaging, RARE for ^{19}F T_2-weighted imaging, and FLASH for ^{19}F T_2*-weighted imaging.

We found that the response of the PFC T_1 and T_2 relaxation rates to SPIO concentration is different than that found for water. For Molday ION, the reported T_1 and T_2 water relaxivities are 36.4 sec^{-1} mM^{-1} and 70.6 sec^{-1} mM^{-1} at 0.47 T, respectively. Since SPIO magnetization is known to saturate at low field strength (24) and ^{1}H and ^{19}F have similar gyromagnetic ratios, we expected similar relaxivities for the PFC formulation. We found that the ^{19}F PFC T_1 was independent of SPIO concentration and the T_2 relaxivity was over 4-times greater that that of water. We also confirmed that the ^{1}H relaxivity of Molday ION at 7 T (75.7 sec^{-1} mM^{-1}) is similar to the low field measurement (data not shown). We hypothesize that, since the PFC is formulated as a nanoemulsion, molecular diffusion is limited by the droplet size, as opposed to rapid and freely diffusing bulk water. Hussain, et al., used an outer sphere relaxation model to describe the effect of molecular diffusion on magnetic-particle related changes to nuclear relaxation (25). They demonstrated that, in viscous systems, slow molecular diffusion enhances the SPIO nanoparticle contribution to the transverse relaxation rate, but reduces the particle contribution to longitudinal relaxation. These results are important for combining SPIO and PFC for cell tracking. First of all, T_1-weighted UTE scans can be used for PFC quantification since T_1 is independent of SPIO concentration. Also, enhanced SPIO T_2 relaxivity facilitates filtering out co-labeled cells in T_2-weighted scans.

MPIO particles are very effective in generating T_2* contrast for cellular MR; thus, it was surprising that MPIO particles were not as effective in reducing the intracellular PFC T_2 as the two other SPIO nanoparticles tested. One explanation could be that MPIO has a lower r_2 than the nanoparticles; however, intracellular distribution of the SPIO and PFC may also be an important factor. Only a few MPIO particles are required for a high intracellular iron content. Compared to a single MPIO particle, it is estimated that ~10^5 ITRI-IOP particles are needed to yield the same 0.5 pg of intracellular iron (13). The TEM images showed that the ITRI-IOP nanoparticles particles were well dispersed and closely coupled with the PFC droplets, whereas the MPIO was not closely associated. The surface chemistry of the particles may also play a role in their association with PFC droplets: MPIO particles consist of an inert polystyrene-divinylbenzene polymer microspheres and ITRI-IOP and Molday ION have PEG and dextran coatings, respectively.

Although the goal of this study was to explore quenching PFC label when cells are co-labeled with SPIO, i.e. in the case of PFC transferred from dead cells to SPIO-labeled macrophages, our findings also revealed that combining PFC and SPIO cell labeling can be used to track two cell populations simultaneously. We used compacted cell pellets to simulate tissues with high-labeled-cell densities and probed the ^{19}F PFC NMR properties and feasibility of ^{19}F imaging. We further diluted the cells 5-fold in agarose to compare the NMR properties in a dilute labeled cell case. In all compacted cell pellets, the fluorine resonance had a greater down-field chemical shift and greater linewidth when compared to the cells diluted 5-fold in agarose. This was expected because the increased SPIO density in the samples results in inhomogeneous line broadening. For mixed populations of PFC-labeled and SPIO nanoparticle labeled cells, the NMR linewidth and chemical shifts were 3–4 fold greater when measured in the cell pellet. For the co-labeled cells, the differences in the NMR lines were even greater for some samples. However, it's difficult to draw conclusions about linewidths and shifts from these results, because cell packing is hard to control and is potentially heterogeneous across the samples. An important result is that the ^{19}F signal in the co-labeled and co-localized labeled cell pellets could be distinguished, providing a basis to develop this technique for *in vivo* applications. A broadened ^{19}F linewidth does not prohibit the ability to image a population of labeled cells, since fluorine imaging is generally carried out at a much lower resolution (>2x lower) than typical ^{1}H imaging to help overcome the lower sensitivity for the dilute ^{19}F probe (23). Thus, with voxel resolutions of greater than a ppm, anatomical localization of labeled cells should not be affected greatly.

We demonstrated *in vivo* imaging of different cell populations with a mouse inflammation model. By timing the injection of PFC and/or SPIO, we aimed to generate labeled macrophage populations with PFC-labeled cells, PFC-labeled cells in proximity to SPIO labeled cells, and PFC/SPIO co-labeled cells. Our imaging results revealed PFC T_2 and T_2* relaxation properties strongly suggesting that we were successful in generating all of these cell populations *in vivo*. To identify PFC-only labeled cells and a population PFC-labeled and SPIO-labeled co-localized cells, we used signal from the iliac lymph nodes. For the PFC/SPIO co-labeled cell population, we did not find PFC signal from the iliac lymph nodes as with the previous experiment. This may be due to injecting too high a dose of Molday

ION and thus generating an ultra-short ^{19}F T_2. Also, since we were focusing on identifying PFC-labeled cells, we did not collect a T_2*-weighted ^{1}H image to confirm the presence of SPIO-labeled cells in the iliac lymph nodes. Instead, we used signal identified as coming from the iliac bone marrow as an example of *in vivo* co-labeled cells, i.e. having a short ^{19}F T_2 and short T_2*.

To the best of our knowledge, this is the first study that explored combining these two cell-labeling techniques for MRI cell tracking. We are aware of only a few other studies with the purpose of detecting of two uniquely labeled cell populations in the same subject (26–28). In these cases, two PFC formulations with distinct ^{19}F chemical shifts were used to separately label cell populations.

Conclusion

Cellular MRI is a powerful technique to visualize the migration and accumulation of cells in deep tissues. Here, we demonstrated the proof-of-concept that, by combining PFC and SPIO cell labeling reagents, one can improve and expand applications of cellular MRI. Systemic labeling of macrophages could be used to quench PFC label transferred from dead cell transplants or both labels could be used to track two cell populations simultaneously and probe cell-cell proximity *in vivo*. Further examples in animal models will be needed to fully explore new applications of this new methodology for MRI cell tracking.

Acknowledgments

The authors gratefully acknowledge Brent Barbe for assisting with the animal experiments, Robert G. Bryant and Yijen L. Wu for helpful discussions, and Joseph Suhan for collecting the TEM images. This work was supported by grants from the National Institutes of Health (NIH), P41 EB001977 and R01-CA134633.

References

1. Ahrens ET, Bulte JW. Tracking immune cells in vivo using magnetic resonance imaging. Nat Rev Immunol. 2013; 13(10):755–763. [PubMed: 24013185]
2. Hong H, Yang YN, Zhang Y, Cai WB. Non-Invasive Imaging of Human Embryonic Stem Cells. Curr Pharm Biotechno. 2010; 11(6):685–692.
3. Youn H, Hong KJ. In vivo non invasive molecular imaging for immune cell tracking in small animals. Immune Netw. 2012; 12(6):223–229. [PubMed: 23396713]
4. Wu, YL.; Ye, Q.; Zhang, H.; Hitchens, TK.; Ho, C. Other Non-Stem Cell Therapies fore Cellular Tracking - Inflammatory Cell Tracking. In: Dara, L.; Kraitchman, JCW., editors. Stem Cell Labeling for Delivery and Tracking Using Noninvasive Imaging. Boca Raton, FL: CRC Press; 2012. p. 335-352.
5. Dodd SJ, Williams M, Suhan JP, Williams DS, Koretsky AP, Ho C. Detection of single mammalian cells by high-resolution magnetic resonance imaging. Biophys J. 1999; 76(1 Pt 1):103–109. [PubMed: 9876127]
6. Shapiro EM, Sharer K, Skrtic S, Koretsky AP. In vivo detection of single cells by MRI. Magnet Reson Med. 2006; 55(2):242–249.
7. Wu YL, Ye Q, Foley LM, Hitchens TK, Sato K, Williams JB, Ho C. In situ labeling of immune cells with iron oxide particles: An approach to detect organ rejection by cellular MRI. P Natl Acad Sci USA. 2006; 103(6):1852–1857.
8. Ahrens ET, Zhong J. In vivo MRI cell tracking using perfluorocarbon probes and fluorine-19 detection. NMR Biomed. 2013; 26(7):860–871. [PubMed: 23606473]

9. Janjic JM, Ahrens ET. Fluorine-containing nanoemulsions for MRI cell tracking. Wires Nanomed Nanobi. 2009; 1(5):492–501.
10. Srinivas M, Morel PA, Ernst LA, Laidlaw DH, Ahrens ET. Fluorine-19 MRI for visualization and quantification of cell migration in a diabetes model. Magn Reson Med. 2007; 58(4):725–734. [PubMed: 17899609]
11. Winter EM, Hogers B, van der Graaf LM, Gittenberger-de Groot AC, Poelmann RE, van der Weerd L. Cell tracking using iron oxide fails to distinguish dead from living transplanted cells in the infarcted heart. Magn Reson Med. 2010; 63(3):817–821. [PubMed: 20187188]
12. Terrovitis J, Stuber M, Youssef A, Preece S, Leppo M, Kizana E, Schar M, Gerstenblith G, Weiss RG, Marban E, Abraham MR. Magnetic resonance imaging overestimates ferumoxide-labeled stem cell survival after transplantation in the heart. Circulation. 2008; 117(12):1555–1562. [PubMed: 18332264]
13. Chen CL, Zhang H, Ye Q, Hsieh WY, Hitchens TK, Shen HH, Liu L, Wu YJ, Foley LM, Wang SJ, Ho C. A new nano-sized iron oxide particle with high sensitivity for cellular magnetic resonance imaging. Mol Imaging Biol. 2011; 13(5):825–839. [PubMed: 20862612]
14. Liu L, Hitchens TK, Ye Q, Wu Y, Barbe B, Prior DE, Li WF, Yeh FC, Foley LM, Bain DJ, Ho C. Decreased reticuloendothelial system clearance and increased blood half-life and immune cell labeling for nano- and micron-sized superparamagnetic iron-oxide particles upon pre-treatment with Intralipid. Biochim Biophys Acta. 2013; 1830(6):3447–3453. [PubMed: 23396002]
15. Hinds KA, Hill JM, Shapiro EM, Laukkanen MO, Silva AC, Combs CA, Varney TR, Balaban RS, Koretsky AP, Dunbar CE. Highly efficient endosomal labeling of progenitor and stem cells with large magnetic particles allows magnetic resonance imaging of single cells. Blood. 2003; 102(3): 867–872. [PubMed: 12676779]
16. Deoni SC, Rutt BK, Peters TM. Rapid combined T1 and T2 mapping using gradient recalled acquisition in the steady state. Magn Reson Med. 2003; 49(3):515–526. [PubMed: 12594755]
17. Girolomoni G, Lutz MB, Pastore S, Assmann CU, Cavani A, Ricciardi-Castagnoli P. Establishment of a cell line with features of early dendritic cell precursors from fetal mouse skin. Eur J Immunol. 1995; 25(8):2163–2169. [PubMed: 7664779]
18. Ahrens ET, Feili-Hariri M, Xu H, Genove G, Morel PA. Receptor-mediated endocytosis of iron-oxide particles provides efficient labeling of dendritic cells for in vivo MR imaging. Magn Reson Med. 2003; 49(6):1006–1013. [PubMed: 12768577]
19. Carr HY, Purcell EM. Effects of Diffusion on Free Precession in Nuclear Magnetic Resonance Experiments. Phys Rev. 1954; 94(3):630–638.
20. Meiboom S, Gill D. Modified Spin-Echo Method for Measuring Nuclear Relaxation Times. Rev Sci Instrum. 1958; 29(8):688–691.
21. Ahrens ET, Flores R, Xu HY, Morel PA. In vivo imaging platform for tracking immunotherapeutic cells. Nat Biotechnol. 2005; 23(8):983–987. [PubMed: 16041364]
22. Ho C, Hitchens TK. A non-invasive approach to detecting organ rejection by MRI: monitoring the accumulation of immune cells at the transplanted organ. Curr Pharm Biotechnol. 2004; 5(6):551–566. [PubMed: 15579044]
23. Hitchens TK, Ye Q, Eytan DF, Janjic JM, Ahrens ET, Ho C. 19F MRI detection of acute allograft rejection with in vivo perfluorocarbon labeling of immune cells. Magn Reson Med. 2011; 65(4): 1144–1153. [PubMed: 21305593]
24. Jung CW, Jacobs P. Physical and chemical properties of superparamagnetic iron oxide MR contrast agents: ferumoxides, ferumoxtran, ferumoxsil. Magn Reson Imaging. 1995; 13(5):661–674. [PubMed: 8569441]
25. Hussain R, Andreyev A, Asi J, Noginova N. Effects of magnetic nanoparticles on nuclear spin relaxation in viscous systems. J Phys D Appl Phys. 2011; 44(43)
26. Partlow KC, Chen J, Brant JA, Neubauer AM, Meyerrose TE, Creer MH, Nolta JA, Caruthers SD, Lanza GM, Wickline SA. 19F magnetic resonance imaging for stem/progenitor cell tracking with multiple unique perfluorocarbon nanobeacons. FASEB J. 2007; 21(8):1647–1654. [PubMed: 17284484]

27. Janjic, JM.; Kadayakkara, DK.; Pusateri, LK.; Ahrens, ET. International Society for Magnetic Resonance in Medicine. Honolulu, HI: 2009. Novel Perfluorocarbon Nanoemulsion for 19F Cell Tracking of Two Cell Populations In Vivo.

28. Kampf T, Fischer A, Basse-Lusebrink TC, Ladewig G, Breuer F, Stoll G, Jakob PM, Bauer WR. Application of compressed sensing to in vivo 3D (1)(9)F CSI. J Magn Reson. 2010; 207(2):262–273. [PubMed: 20932790]

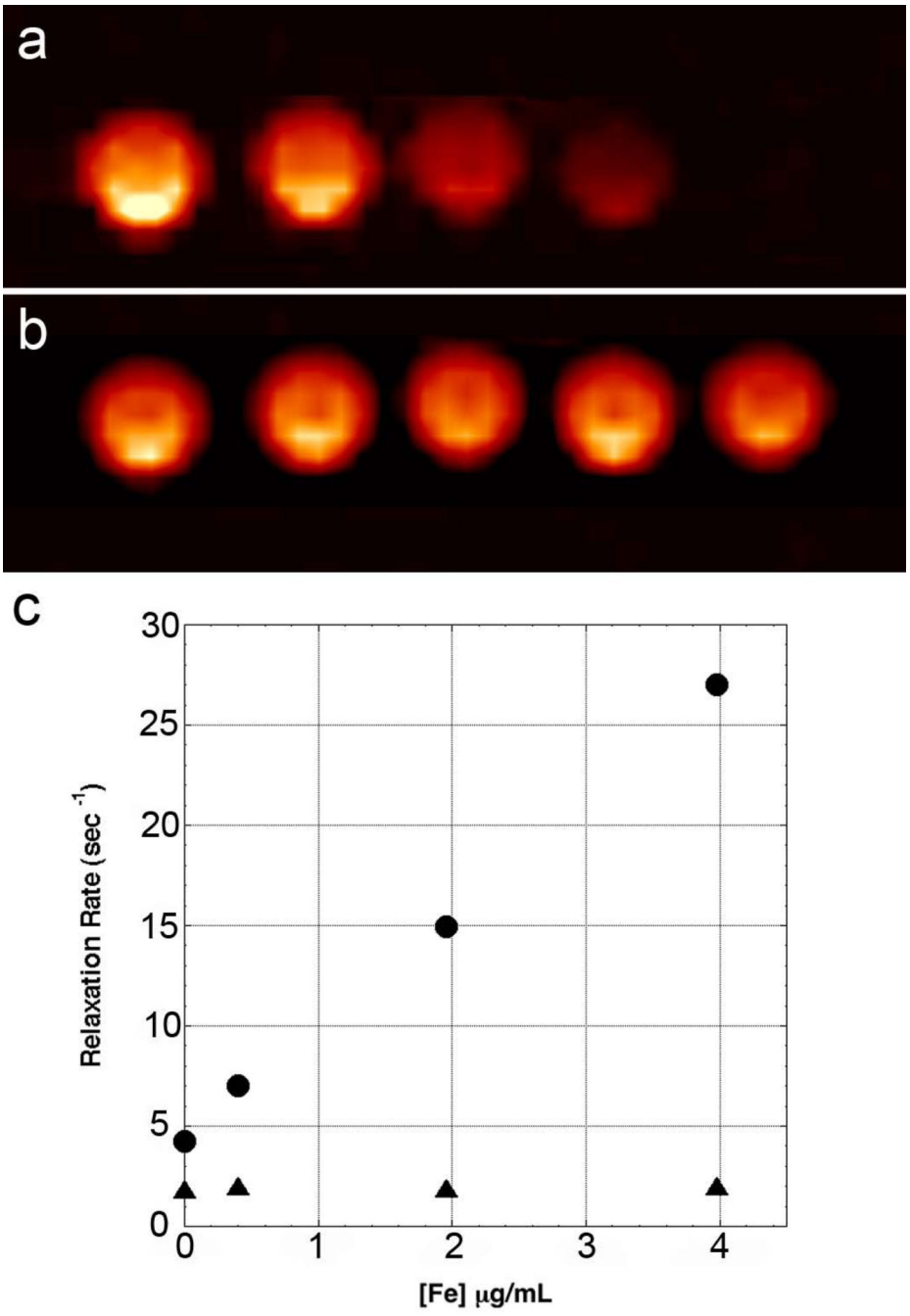

Figure 1.

^{19}F images and relaxation rates for PCF/ Molday ION mixtures. Panel a shows a ^{19}F T_2-weighted spin-echo (TE = 70 ms) image of PFC phantoms containing SPIO at concentrations of 0, 0.4, 2, 4, and 20μg Fe/mL (left to right). ^{19}F images are shown in pseudo color (hot iron scale) to distinguish them from standard ^{1}H images. Panel b shows a ^{19}F UTE3D image (TE = 20μs) for the same phantoms. Panel c shows a plot of relaxation rates, R_2 (circles) and R_1 (triangles), versus iron concentration. A regression of R_2 versus iron concentration for these 4 points gives a slope of 5.65 sec^{-1} μg^{-1} mL (R=0.999). Data

for the phantom containing 20 μg Fe /mL is not shown on the plot. The R_1 was measured to be 2.08 sec^{-1} and R_2 was rapid, estimated to be approximately 166 sec^{-1}.

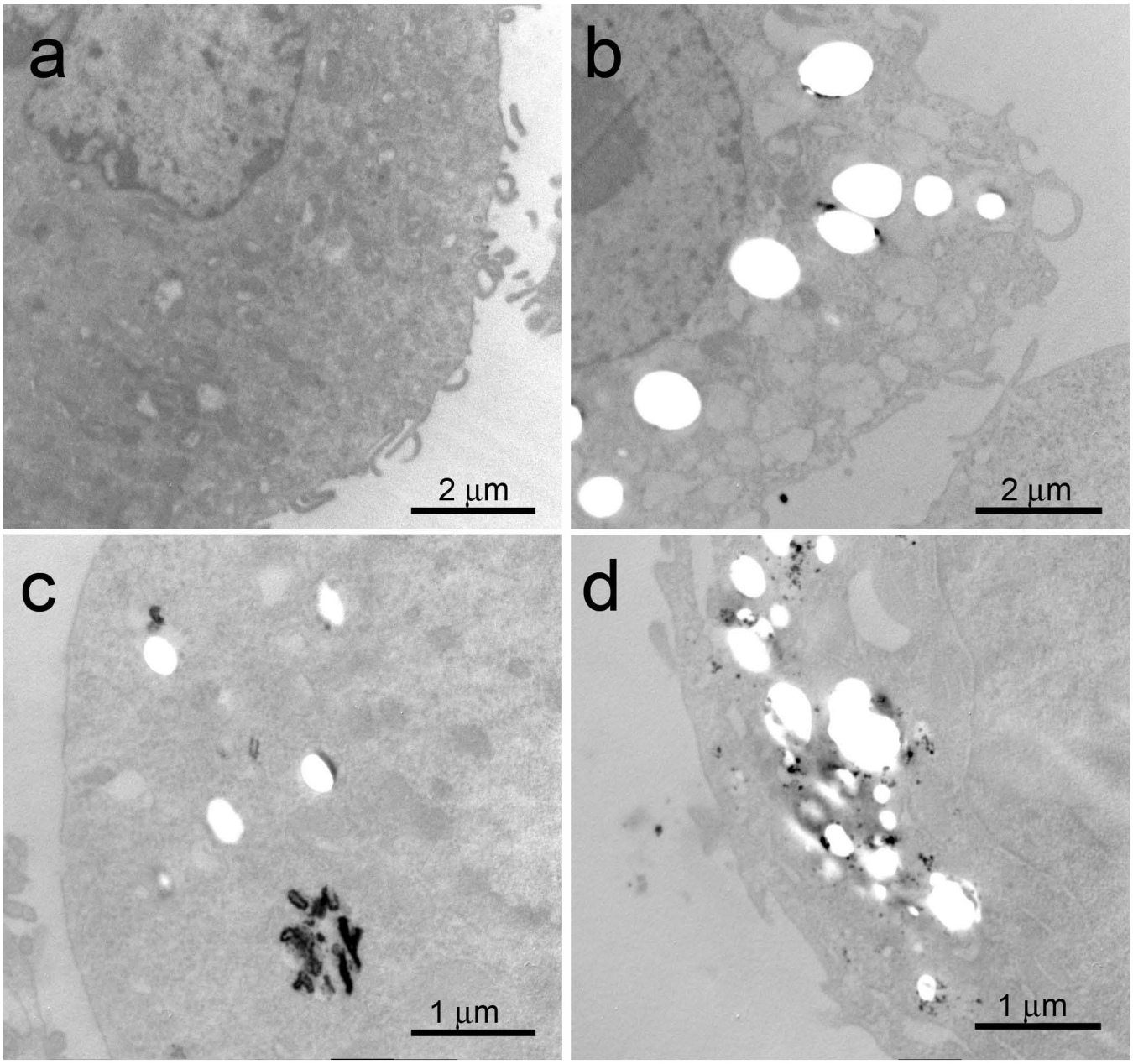

Figure 2.

TEM images of FSDC's labeled with PFC and co-labeled with either micron-sized or nano-sized SPIO particles. Panels a and b unlabeled and PFC-labeled FSDC cells, respectively. The white spots seen in B are the fluorine nanoemulsion droplets. Panel c shows TEM of a PFC/MPIO co-labeled cell. A micron-sized SPIO particle is seen in the center of the lower part of the image. Panel d shows a cell co-labeled with PFC and ITRI-IOP. Many spots of high electron density due to the nano-sized SPIO particles are seen associated with or in close proximity to the PFC droplets.

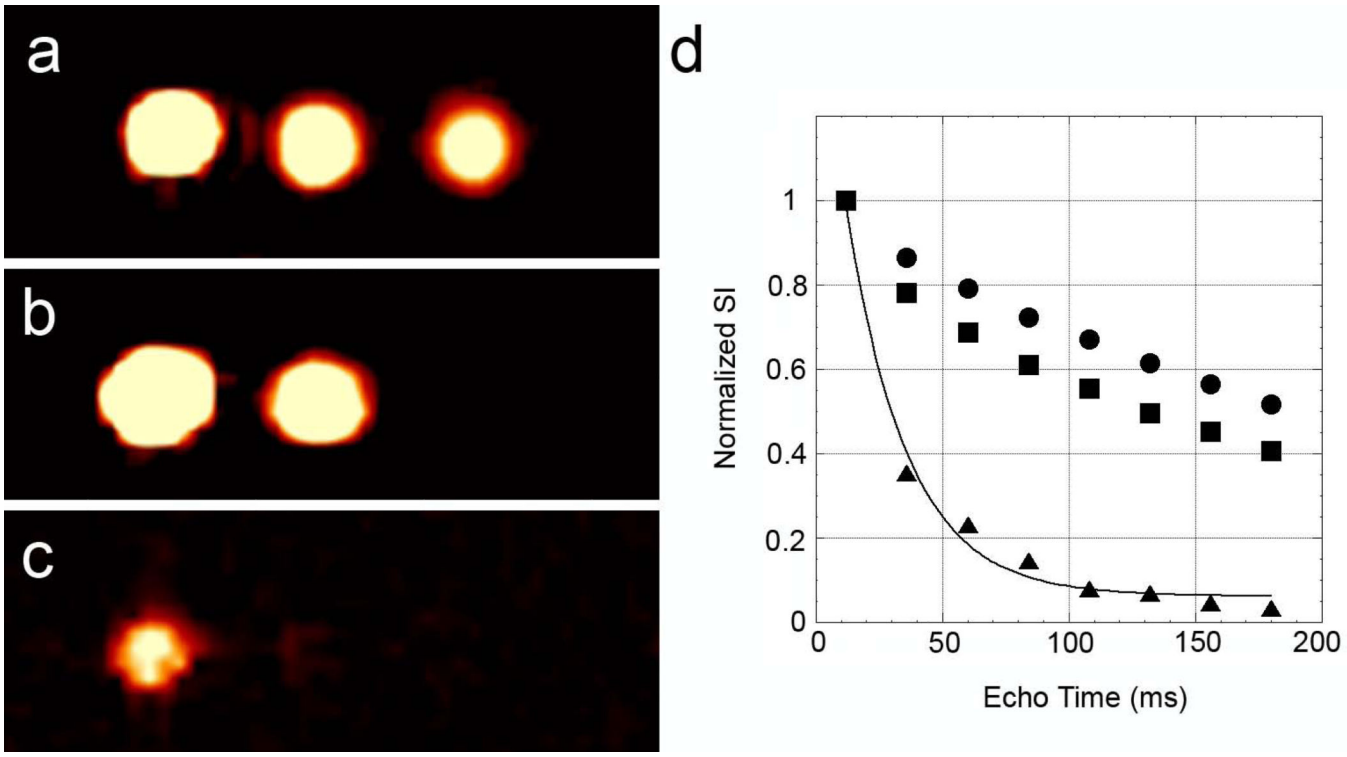

Figure 3.

Selective ^{19}F Imaging PFC/SPIO labeled cell pellets. Panel a shows a spin-density weighted UTE3D image (TR = 20 μs) of three cell pellets: PFC labeled (left), an equal mixture of PFC labeled cells and ITRI-IOP labeled cells with 0.45 pg Fe/cell (middle), and PFC/ITRI-IOP co-labeled cells with 0.56 pg Fe/cell (right). Panel b shows a RARE image (TE = 84 ms) of the three cell pellets, demonstrating negative selection for the co-labeled cells. Panel c shows a FLASH image (100/1 ms TR/TE) of the three cell pellet samples demonstrating negative selection for samples containing SPIO labeled cells. Panel d shows a plot of normalized signal versus echo time for a series of RARE images for the PFC-labeled cells (circles), the mixture of PFC and SPIO labeled cells (squares), and PFC/SPIO co-labeled cells (triangles). An exponential decay is plotted through the signal from the co-labeled cells showing a T_2 of 23 ms.

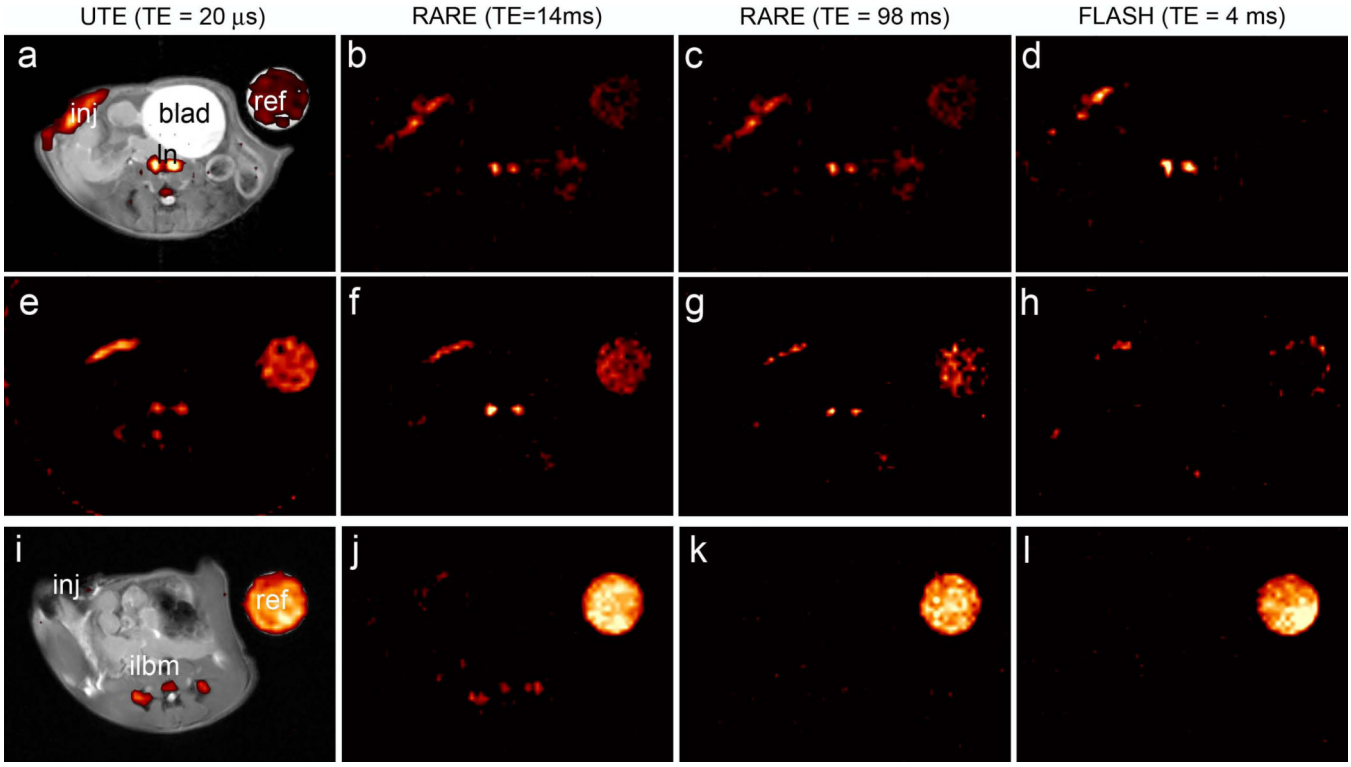

Figure 4.

Preliminary study for detecting PFC labeled cells in the presence of SPIO labeled cells and PFC/SPIO co-labeled cell populations in vivo. Each row shows images collected during the same session. Columns are ^{19}F images from UTE3D (TE = 20 μs), a short-TE RARE (TE = 14 ms), a long-TE RARE (TE = 98 ms), and FLASH (TE = 4 ms), left to right, respectively. Panel a shows a $^{19}F/^{1}H$ composite image 5 days following surgical injury and injection of PFC. The ^{19}F image was collected with a UTE3D. The surgical injury (inj), bladder (blad) iliac lymph nodes (ln) and fluorine reference tube (ref) are labeled as indicated. The short-TE RARE (b), long-TE RARE (c) and FLASH (d) demonstrate that the PFC has a long T_2 and long T_2*. Panels in the second row (e-h) show the corresponding images two days following a subsequent MOLDAY ION injection. Observation of the strong signal from the lymph nodes in the long-TE RARE (g) and not in the FLASH (h) demonstrates that the PFC has a long T_2, but short T_2*. Panels in the 3rd row (i-l) are from a mouse give PFC and SPIO simultaneously following surgical injury. In the composite image (i), the surgical injury site, reference tube, signal from the iliac bone marrow (ilbm) are indicated. The short-TE RARE image (j) shows reduced signal. Fluorine signal is also absent in the long-TE RARE (k) and FLASH (l) images, demonstrating that the PFC has a short T_2 and short T_2*.

Table 1

^{19}F NMR Properties of PFC labeled Cells in Agarose. Each sample contained 6×10^6 labeled FSDC cells diluted 5x in agarose to a final volume of 100 μL. Row entries 2–4, 9–10, and 13–14 had two cell populations of 3×10^6 each, with one population labeled with PFC and the other labeled with SPIO as indicated. Rows 1, 5–8, 11–12, and 15–16 show data from a single population of ^{19}F-labeled or co-labeled cells. Iron concentration was measured with ICP-MS. The NMR shift is relative to the reference PFC-labeled cells. The shift and line width (FWHH) were estimate from the NMR spectrum and the T_2 was measured with a CPMG pulse sequence. T_2 was not measured in samples with very broad lines.

	Cell Pop. 1 Label	Cell Pop. 2 Label	[Fe]/cell	NMR Shift	NMR Line Width	T_2
1	PFC		---	---	200 Hz	220 ms
2	PFC	ITRI-IOP	0.45 pg	0.5 ppm	450 Hz	220 ms
3	PFC	ITRI-IOP	1.8 pg	0.5 ppm	600 Hz	194 ms
4	PFC	ITRI-IOP	4.2 pg	0.6 ppm	650 Hz	195 ms
5	PFC and ITRI-IOP		0.39 pg	0.5 ppm	1.7 kHz	35 ms
6	PFC and ITRI-IOP		0.59 pg	0.5 ppm	3 kHz	20 ms
7	PFC and ITRI-IOP		2.0 pg	0.65 ppm	4.6 kHz	~1ms
8	PFC and ITRI-IOP		6.2 pg	0.65 ppm	7 kHz	--
9	PFC	Molday ION	3.2 pg	0.3 ppm	500 Hz	220 ms
10	PFC	Molday ION	5.9 pg	0.3 ppm	500 Hz	215 ms
11	PFC and Molday ION		3.0 pg	0.3 ppm	6.2 kHz	--
12	PFC and Molday ION		4.9 pg	0.3 ppm	8 kHz	--
13	PFC	MPIO	3.2 pg	0.2 ppm	400 Hz	196 ms
14	PFC	MPIO	5.0 pg	0.6 ppm	440 Hz	206 ms
15	PFC and MPIO		2.8 pg	0.25 ppm	1.2 kHz	140 ms
16	PFC and MPIO		4.2 pg	0.35 ppm	2.1 kHz	120 ms